Asian Journal of Chemistry; Vol. 33, No. 6 (2021), 1309-1318

ASIAN JOURNAL OF CHEMISTRY

https://doi.org/10.14233/ajchem.2021.23176

Synthesis and Evaluation of Fe(III) Embedded Silane Grafted Layered Double Hydroxide with Reduced Graphene Oxide Support as an Efficient Adsorbent for V(V) and Se(IV) from Aqueous Systems

S. SUMA[1], S. SEEMA[1], S.V. MANOJ[1], V.S. SUMI[2] and S. RIJITH[1,*]

[1]Post Graduate and Research Department of Chemistry, Sree Narayana College (Affiliated to University of Kerala, Trivandrum), Kollam-691001, India

[2]Department of Chemistry, Government College, Attingal-695101, India

*Corresponding author: E-mail: rijithsreenivas@gmail.com

Received: 20 February 2021; *Accepted*: 3 April 2021; *Published online*: 5 June 2021; AJC-20361

The objectives of present work emphasize the successful usage of Fe(III) modified layered double hydroxide clays with reduced graphene support (Si-rGO/LDH-Fe) for the removal of V(V) and Se(IV) from aqueous systems. The precursors along with the modified and sorbent loaded materials were successfully characterized by BET surface area analyzer, SEM-EDS mapping, FTIR, potentiometric titrations and XPS analysis. Sorption performance of Si-rGO/LDH-Fe towards V(V) and Se(IV) under optimized conditions such as pH, temperature and concentration were investigated. The equilibrium and kinetic investigations revealed that the adsorption of V(V) and Se(IV) onto Si-rGO/LDH-Fe follows non-linear Langmuir isotherm and pseudo-second-order model, respectively. The equilibrium reached within 120 min and the Langmuir isotherm fit well with the experimental data. The adsorption mechanism was proposed to be ligand exchange with electrostatic interactions. Such results indicated that V(V) and Se(IV) species interact by the protonated hydroxyl moieties on the surface of Si-rGO/LDH-Fe. The practical efficacy and effectiveness of Si-rGO/LDH-Fe was also compared with some of the related works reported so far. The regeneration capacity and reusability of Si-rGO/LDH-Fe were also tested by employing four cycles of desorption experiments.

Keywords: Vanadium, Selenium, Graft copolymerization, Adsorption kinetics, Isotherm, Desorption.

INTRODUCTION

Industrialization as well as urbanization has raised the problem of heavy metal pollution in natural water resources. Vanadium and selenium are toxic and carcinogenic elements at higher concentrations [1,2], which enter to the aqueous system *via* natural exogenic and endogenic activities and also from the discharge of agricultural wastewater, steel and paper industries [3,4]. The discharge limit of V(V) and Se(IV) are reported to be 50 µg/L and 10 µg/L as per China's Drinking Water Standard (GB 5749-2006) and World Health Organization standard (WHO), respectively [5,6]. Various technologies have adopted by many researchers to immobilize the toxic oxy-anions of vanadium and selenium. Among these techniques adsorption bags much appreciation because it is economically feasible, convenient and has high rate of removal efficiency even at low concentration [7]. Therefore, the removal of these pollutants is imperative in wastewater treatment.

Iron oxyhydroxide nanoparticles are known to have strong affinity towards the various oxoanionic pollutants owing to their high surface to volume ratio, dispersity, biocompatibility, high selectivity and ubiquitous nature [8]. The use of nano-materials as a template for iron oxyhydroxide can effectively control its particle size, dispersion and aggregation, thereby increasing the adsorption efficiency. The conventional 2D materials such as layered double hydroxide (LDH) and graphene have been reported as potential adsorbents for toxic oxy anions [9,10]. LDH also known as hydrotalcite like compound of general formula $[M^{2+}_{1-p}M^{3+}_{p}(OH)_2]^{p+}[(A^{q-})_{p/q}]^{p-}\cdot y\,H_2O$, have been proved as one of the most favourable material owing to its versatile nature, simple method of preparation and low cost [11,12]. The LDH based composites can offer dramatically inflated properties than indigenous polymer matrices. Silane grafting improves the compatibility between LDH and the polymer backbone, which facilitates enhanced surface properties of the polymer composite [13].

Graphene and its derivatives have been reported as building blocks for the fabrication of hybrid materials that can exhibit comparatively higher performances towards adsorption [14]. Graphene oxide (GO) contains many oxygen rich moieties, which repels anionic species [15]. Reduced graphene oxide (rGO) on the other hand shows better efficiency towards anionic pollutants. Both rGO and LDH nanosheets have to overcome the common problem of aggregation in their practical applications [16,17]. LDH can avoid coagulation of graphene whereas graphene stabilizes the layer structure and enhance the surface activity of LDH in their combined composite form [18]. These drawbacks can be dealt with a combination of LDH and rGO into a multifunctional hierarchical composite material with extra ordinary properties. Consequently, it is highly anticipated that the obtained 3D hierarchical composite material can greatly enhance the adsorption efficiency towards oxyanions.

In this work, a novel iron(III) modified layered double hydroxide clay with reduced graphene support (Si-rGO/LDH-Fe) was prepared from LDH and rGO *via* emulsion polymerization and its application for the removal of V(V) and Se(IV) was evaluated. The morphological and structural characteristics of Si-rGO/LDH-Fe composite was systematically investigated by using zeta potential, BET, FTIR, XPS and SEM-EDS elemental mapping analysis. Batch adsorption experiments were performed using Si-rGO/LDH-Fe to immobilize V(V) and Se(IV) oxyanions under different experimental conditions. The kinetics and equilibrium isotherm parameters for sorption of V(V) and Se(IV) onto Si-rGO/LDH-Fe was evaluated and the possible sorption mechanisms were also proposed. The prepared composite material (Si-rGO/LDH-Fe) with a unique structural and surface properties exhibit excellent adsorption capacity towards V(V) and Se(IV). The enhanced sorption potential of Si-rGO/LDH-Fe illustrates a promising alternate candidate in wastewater treatment process.

EXPERIMENTAL

All chemicals used in the present work were of analytical grade and all the solutions were prepared with deionized water. Graphite powder and D-glucose anhydrous used as precursors and reducing agent, respectively for the preparation of reduced graphene oxide (rGO) were purchased from E-Merck India Ltd. AR grade $Mg(NO_3)_2{\cdot}6H_2O$ and $Al(NO_3)_3{\cdot}9H_2O$, tetraethyl orthosilicate (TEOS), sodium dodecylbenzene sulfonate (SDBS), $FeCl_3{\cdot}6H_2O$ and HCl (37%) were also purchased from E-Merck, India Ltd., while ethylene glycol dimethacrylate (EGDMA) and acrylic acid were procured from Fluka Chemie (Switzerland). AR grade $NaVO_3$ and Na_2SeO_3 (Aldrich) were dissolved in deionized water to obtain the stock solution of V(V) and Se(IV), respectively. Working solutions were prepared by the successive dilution of the stock solutions of V(V) and Se (IV).

Synthesis of Si-rGO/LDH-Fe: The precursors such as GO and LDH were synthesized by modified Hummer's method and coprecipitation method, respectively [19,20]. Graphene oxide (GO) is converted to reduced graphene oxide (rGO) by glucose reduction method [21]. Emulsion polymerization followed by crosslinking was employed for the fabrication of Si-rGO/LDH-Fe. Briefly, 10.0 g of LDH was dispersed in 100 mL methanol and the mixture was agitated thoroughly for 30 min, in which 0.20 g of SDBS was added under N_2 atmosphere for anion exchange reactions. During the surface modification, 7.0 g of LDH was stirred with 50 mL methanol and 3.0 g TEOS for 48 h at room temperature. The suspension was undergo polymerization reaction initiated by potassium persulfate at 70 ºC with acrylic acid as monomer and EGDMA as crosslinker for 24 h. During the polymerization reaction, 0.2 g rGO was introduced and N_2 gas purged throughout the reaction. The obtained polymer (Si-rGO/LDH) was washed with deionized water to remove excess monomers and homopolymers *via* sonication. Subsequently, Fe(III) modified polymer composite was prepared by adding 10.0 g Si-rGO/LDH in 100 mL deionized water with 0.20 g $FeCl_3{\cdot}6H_2O$ under acidic condition, the suspension was stirred for 3 h at 60 ºC. The resultant composite material (Si-rGO/LDH-Fe) was separated, washed with deionized water and finally dried at 50 ºC.

Characterization: In order to investigate the surface features along with the sorption properties of the materials used throughout the experiments were carried out by FTIR, SEM-EDS, XPS, zeta potential and BET analysis. The functional groups associated with the samples were identified using Perkin-Elmer IR-180 spectrophotometer worked at a range of 4000-500 cm^{-1}. Investigation on the surface morphology and elemental analysis of the samples were carried out using Philips XL 30 CP scanning electron microscope coupled with an energy dispersive X-ray analyzer. The specific surface area, pore size and pore distribution of Si-rGO/LDH-Fe was measured by N_2 adsorption-desorption at 77 K using Brunauer-Emmett-Teller (BET) methods by employing Autosorb IQ-MP system. The residual concentration of V(V) and Se(IV) after adsorption experiments were determined by inductive coupled plasma atomic emission spectroscopy (Perkin Elmer, Aveo 200). The surface charge of materials was measured by using Horida SZ 100 Zeta Sizer zeta potential analyser. The adsorption mechanism and surface binding state of adsorbate onto Si-rGO/LDH-Fe were characterized using Thermo scientific ESCA LAB 250Xi using Al Kα (1048 eV radiation) and peaks were deconvoluted using Gaussian (80%)-Lorentzian curve fitting program, XPS peak fit, version 4.1 with nonlinear background. The isotherm and equilibrium kinetics studies were performed on a temperature-controlled water bath shaker (Labline Instruments Ltd., India) with temperature tolerance of ± 1 ºC.

Sorption experiments: Batch adsorption experiments of V(V) and Se(IV) were conducted in a 250 mL Erlenmeyer flask each containing 50 mL of working solutions on a temperature controlled water bath shaker with an agitation speed of 200 rpm. Batch adsorption experiments were conducted to optimize the sorption performance of Si-rGO/LDH-Fe towards V(V) and Se(IV) sorption at variable operating conditions such as adsorbent dosage, initial pH, contact time, initial concentration and temperature.

The optimization of pH was carried out by equilibrating 0.1 g of Si-rGO/LDH-Fe with known metal ion concentrations maintained at a pH range from 2.0-10.0. The initial pH of solutions was adjusted using 0.1 M HCl or 0.1 M NaOH. At the equilibrium was reached, the solutions were filtered through

0.45 µm membrane filter and the residual concentration of metal ions were determined using ICP-AES. The removal efficiency (η) and adsorption capacity (q_e) were determined by using the following equations:

$$\eta = \frac{C_o - C_e}{C_o} \times 100 \quad (1)$$

$$q_e = \frac{(C_o - C_e)V}{m} \quad (2)$$

where C_o and C_e (mg/L) are the initial and equilibrium concentrations of V(V) and Se(IV) in aqueous solutions, respectively. 'V' is the volume (mL) of the adsorbate solution and 'm' (mg) is the mass of Si-rGO/LDH-Fe used.

Adsorption isotherm: The adsorption isotherm experiments were carried out with 0.1 g of the adsorbent equilibrated with metal ion solutions of concentrations ranging from 50-250 mg/L. To investigate the influence of contact time on the adsorption of metal ions, the supernatant solutions were collected at predetermined time intervals ranging from 0-600 min. The effect of adsorbent dosage on the adsorption of V(V) and Se(IV) were examined by changing the adsorbent dose from 0.1-0.5 g/L for 100 mg/L solutions at a pH of 5.5 and 5.0, respectively.

Recyclability: To examine the regeneration and reusability of Si-rGO/LDH-Fe, cyclic adsorption-desorption experiments were performed using 0.01 M NaOH as desorbing agent. The V(V) and Se(IV) loaded Si-rGO/LDH-Fe were dispersed separately into desorbing medium and shaken for 30 min at 200 rpm at 303 K. The regenerated Si-rGO/LDH-Fe was used for the successive adsorption/desorption cycles.

$$\text{Desorption (\%)} = \frac{\text{Amount of V(V) or Se(IV) desorbed}}{\text{Amount of V(V) or Se(IV) adsorbed}} \times 100 \quad (3)$$

RESULTS AND DISCUSSION

Physico-chemical characterization: The N_2 adsorption-desorption isotherm and pore distribution of Si-rGO/LDH-Fe is presented in Fig. 1. According to the IUPAC classification, the plots for Si-rGO/LDH-Fe exhibited type IV isotherm with an obvious H_3 hysteresis loop at relatively high pressure (P/P_0 > 0.8), implying a well-developed mesoporous architecture [22]. The BJH pore size distribution plot clearly displays the average pore diameter ranges from 2-40 nm, which further supports the structure of Si-rGO/LDH-Fe was mainly composed of mesopores [23]. The BET surface area of Si-rGO/LDH-Fe (128.56 m^2/g) was found to be superior that of precursors such as LDH (22.3 m^2/g) and rGO (39.6341 m^2/g) [10,14]. The high surface area of Si-rGO/LDH-Fe is due to its 3D hierarchical structure assembled from uniformly cross-linked 2D sheets of rGO and LDH, which facilitate rapid mass transfer and fast adsorption towards oxy anionic species.

Zeta-potentials of rGO, rGO-LDH, Si-rGO/LDH and Si-rGO/LDH-Fe were tested at different pHs to illustrate the surface characteristics and the surface interaction in sorption process. As shown in Fig. 2, the zeta potential values of rGO, rGO-LDH, Si-rGO/LDH and Si-rGO/LDH-Fe were -32.83, -28.18, -10.4 and -2.3 mV, respectively at a pH of 5.7. At pH < 5.7, all the

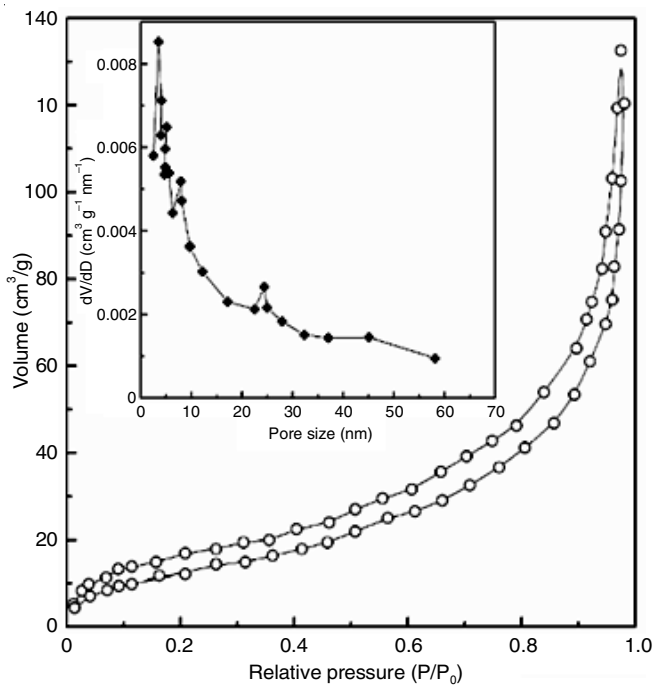

Fig. 1. N_2 adsorption-desorption isotherm and the corresponding pore size distribution of Si- rGO/LDH-Fe

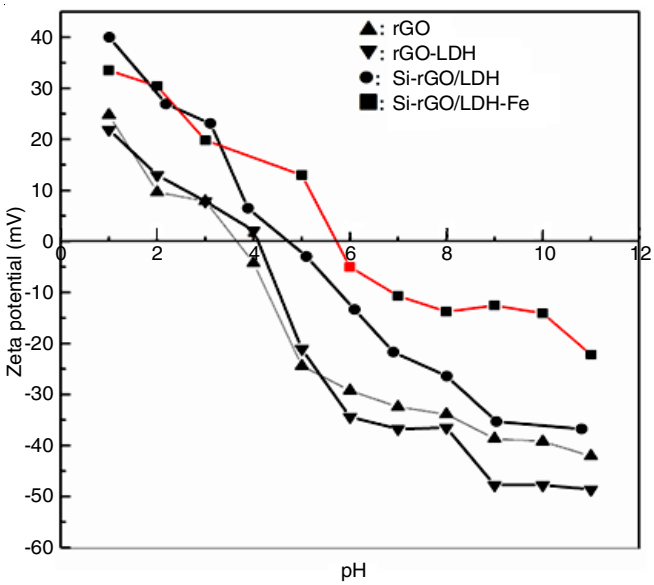

Fig. 2. Zeta potential of rGO, rGO-LDH, Si-rGO/LDH and Si-rGO/LDH-Fe

samples exhibit positive surface potential values. The increasing trend indicates the dissipation of negative charges on the surface during the successive modification process. The negative zeta potential value of Si-rGO/LDH-Fe above the pH 5.7, describes its stability and recyclability in basic medium.

The surface functional groups responsible for the adsorption of V(V) and Se(IV) was evaluated using FTIR analysis. Fig. 3 shows the FTIR spectrum of Si-rGO/LDH-Fe, V(V)-loaded Si-rGO/LDH-Fe and Se(IV)-loaded Si-rGO/LDH-Fe. In all the spectrum, a broad peak observed between 3500-3200 cm^{-1} ascribed the stretching vibrations of hydroxyl group from adsorbed water present in the iron oxy hydroxide and brucite layer of LDH associated with the Si-rGO/-LDH-Fe [24]. FTIR

spectrum of Si-rGO/LDH-Fe (Fig. 3a) exhibited two peaks centred at 1580 and 2983 cm^{-1} ascribed to C=C skeletal and C-H stretching vibrations, respectively from the graphitic domain which indicate the existence of rGO in the composite material [25]. In addition, a prominent peak centred at 1645 cm^{-1} indicated the bending modes of adsorbed water molecules in Si-rGO/LDH-Fe. The vibrational band centred at 996 cm^{-1} attributed the stretching vibration of Si-O-M moieties, which demonstrate silane has been effectively grafted to LDH surface *via* condensation reaction [26]. The intercalation of anions between the LDH layers was confirmed by the characteristic S=O antisymmetric stretching vibrations observed at 1216 cm^{-1} [27]. The peaks at 1447 and 1720 cm^{-1} corresponds to the asymmetric stretching vibrations of carboxylate anion and ester carbonyl groups, respectively which confirms the effective polymerization and crosslinking reactions. Moreover, a prominent peak appeared at 1388 cm^{-1} illustrates the bending vibrational modes of C-OH group from acrylic acid grafted on to LDH surface. The new peaks appeared at 578 cm^{-1} in the spectrum of Si-rGO/LDH-Fe demonstrates the characteristic Fe-O stretching vibrations and it further confirmed by the presence new peaks Fe-OH stretching vibrations at 1045 and 1120 cm^{-1} [28]. After the sorption of V(V) (Fig. 3b), the peaks due to hydroxyl stretching and bending vibrations were shifted from 3412 to 3382 cm^{-1} and 1645 to1634 cm^{-1}, respectively, indicating the involvement of surface hydroxyl group on the adsorption process of V(V). A peak at 578 cm^{-1} in Si-rGO/LDH-Fe was shifted to 558 cm^{-1} in V(V)-loaded Si-rGO/LDH-Fe illustrates the significant role of Fe-OH groups in the adsorption process. Moreover, new peaks appeared at 950 and 824 cm^{-1} ascribed the V=O symmetric stretching vibrations and V-O-V bridging vibrations clearly illustrates the effective adsorption of V(V) onto Si-rGO/LDH-Fe [3]. In the spectrum of Se(IV)-loaded Si-rGO/LDH-Fe (Fig. 3c), shows a characteristic peak appeared at 849 cm^{-1} was attributed to the symmetric Se-O stretching vibrations arise from

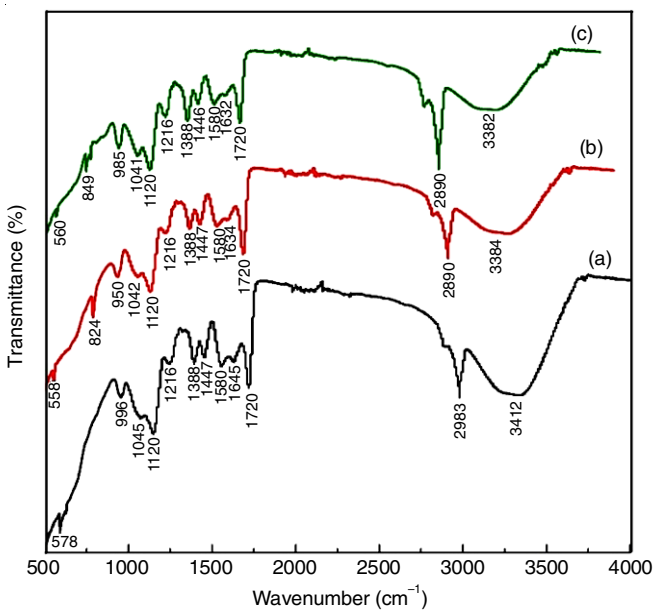

Fig. 3. FTIR spectra of (a) Si-rGO/LDH-Fe (b) V(V)-loaded Si-rGO/LDH-Fe (c) Se(IV)-loaded Si-rGO/LDH-Fe

$HSeO_3^-$ groups. In addition, the OH stretching vibrations arising from Si-rGO/LDH-Fe was shifted from 3412 cm^{-1} to 3382 cm^{-1} in Se(IV)-loaded Si-rGO/LDH-Fe, which confirmed the sorption of $HSeO_3^-$ onto Si-rGO/LDH-Fe *via* ligand exchange with inner sphere surface complexation [29].

X-ray electron spectroscopy was used to explore the distribution and speciation of elements across the Si-rGO/LDH-Fe surface before and after adsorption of V(V) and Se(IV). To gain more insight, wide scan spectra of Si-rGO/LDH-Fe (Fig. 4a) shows the characteristic binding energy values of Mg, Al, Si, O, C and Fe in the XPS analysis. A significant peak observed at 283.2 eV corresponds to C1S revealed the presence of rGO in the composite material. The peaks observed at 1302.8 and 72.7 eV indicating the formation of MgO and Al_2O_3, respectively [30]. A strong signal appeared at 530.57 eV mainly caused by the surface hydroxyl group of Fe(III) oxide and LDH, which illustrates iron has been significantly loaded on to LDH. The silane grafting on LDH was confirmed by the appearance of characteristic peak of Si at 101.5 eV in the wide scan spectra of Si-rGO/LDH-Fe. Characteristic new peaks of V(V) at 516.8 eV and Se(IV) at 56.79 eV in the wide scan spectrum of V(V)-loaded Si-rGO/LDH-Fe and Se(IV)-loaded Si-rGO/LDH-Fe, respectively in Fig. 4b and 4c. The deconvoluted spectra of V $2p_{3/2}$ (Fig. 4d) shows three peaks centred at 519.1, 517.2 and 515.4 eV ascribed the V(V), VO_2 and V_2O_3, respectively, confirmed the quantitative loading of V(V) over the Si-rGO/LDH-Fe surface [31]. In the high-resolution spectra of Se_{3d}, two characteristic satellite peaks located at 55.6 and 59.2 eV with a spin orbital splitting confirm the formation of Fe-$HSeO_3$ complex [32].

The surface morphologies and elemental distribution of Si-rGO/LDH-Fe, V(V)-loaded Si-rGO/LDH-Fe and Se(IV)-loaded Si-rGO/LDH-Fe samples were examined by SEM-EDS analysis. The SEM image of Si-rGO/LDH-Fe (Fig. 5a) displays a 3D porous hierarchical structure in which rGO was embedded between LDH layers decorated with iron oxyhydroxide. The distribution of iron oxide on the surface of polymer composite effectively prevents the agglomeration, hence enhancing the sorption capacity and stability of polymer composite. The EDS elemental mapping displayed the loading of Fe(III) on the surface of Si-rGO/LDH, which designated it as a good sorbent material. Si-rGO/LDH acts as a template for Fe(III) moieties, which provide abundant sorption sites for V(V) and Se(IV). The SEM images of Si-rGO/LDH-Fe after sorption with metal ions are presented in Fig. 5a and 5b. After the V(V) and Se(IV) loading, the pores of Si-rGO/LDH-Fe appeared on its surface exhibit smoother surface with fewer dimension which indicated the surface complexation of Fe(III) species with metal ions. The EDS elemental mapping (Fig. 5a-h) displayed the unique distribution of C, O, Mg, Al, Fe, Se and V on the surface of Si-rGO/LDH-Fe, which illustrate the surface rigidity with enhanced sorption potential.

Effect of pH: It has been widespread consensus that pH is one of the imperative parameters governing the adsorption of metal ions at the solid-liquid interface. The pH of a solution not only influence the speciation of metal ions, but also defines the surface charge and hydroxyl dissociability of Si-rGO/LDH-

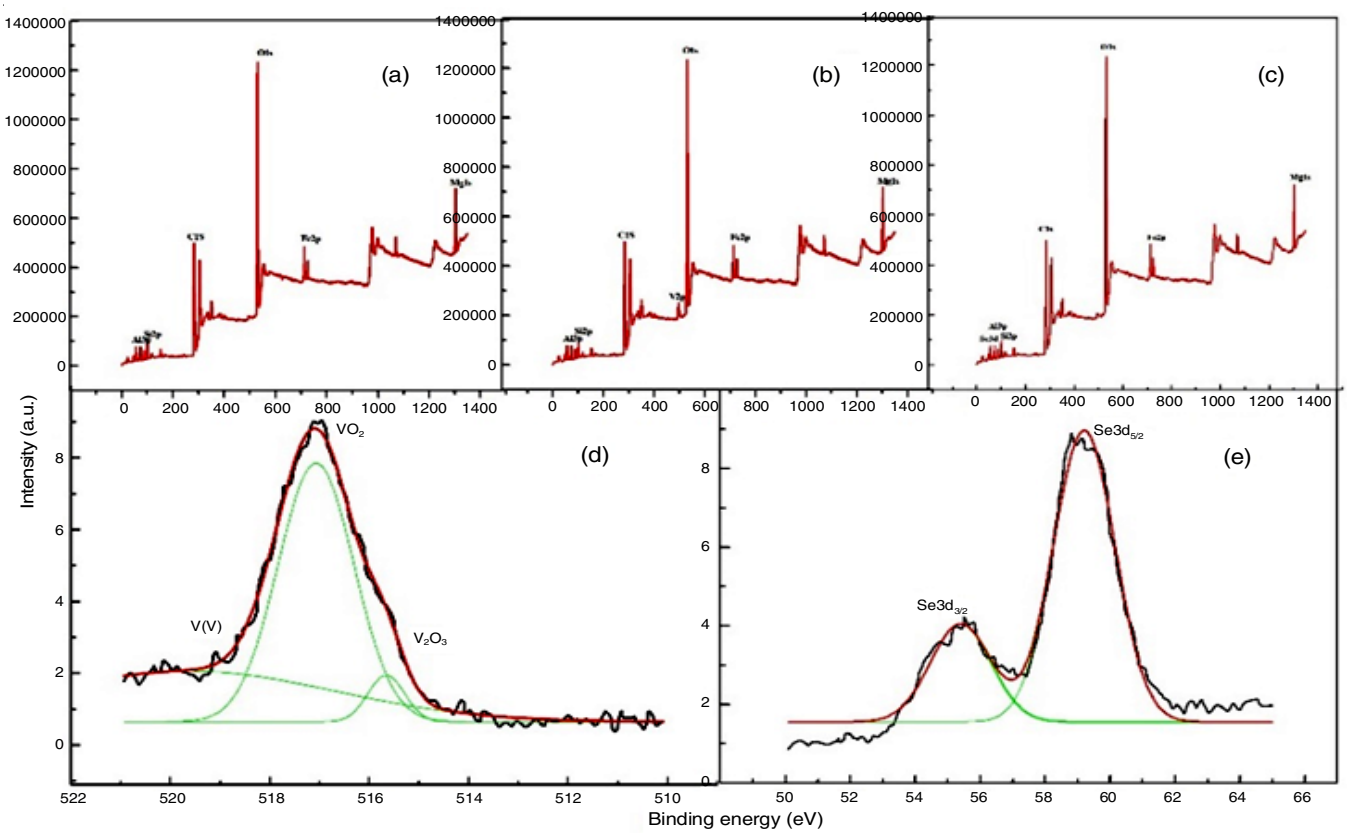

Fig. 4. XPS survey spectra of (a) Si-rGO/LDH-Fe (b) V(V)-loaded Si-rGO/LDH-Fe (c) Se(IV)-loaded Si-rGO/LDH-Fe. High resolution XPS spectra of (d) V2p and (e) Se3d

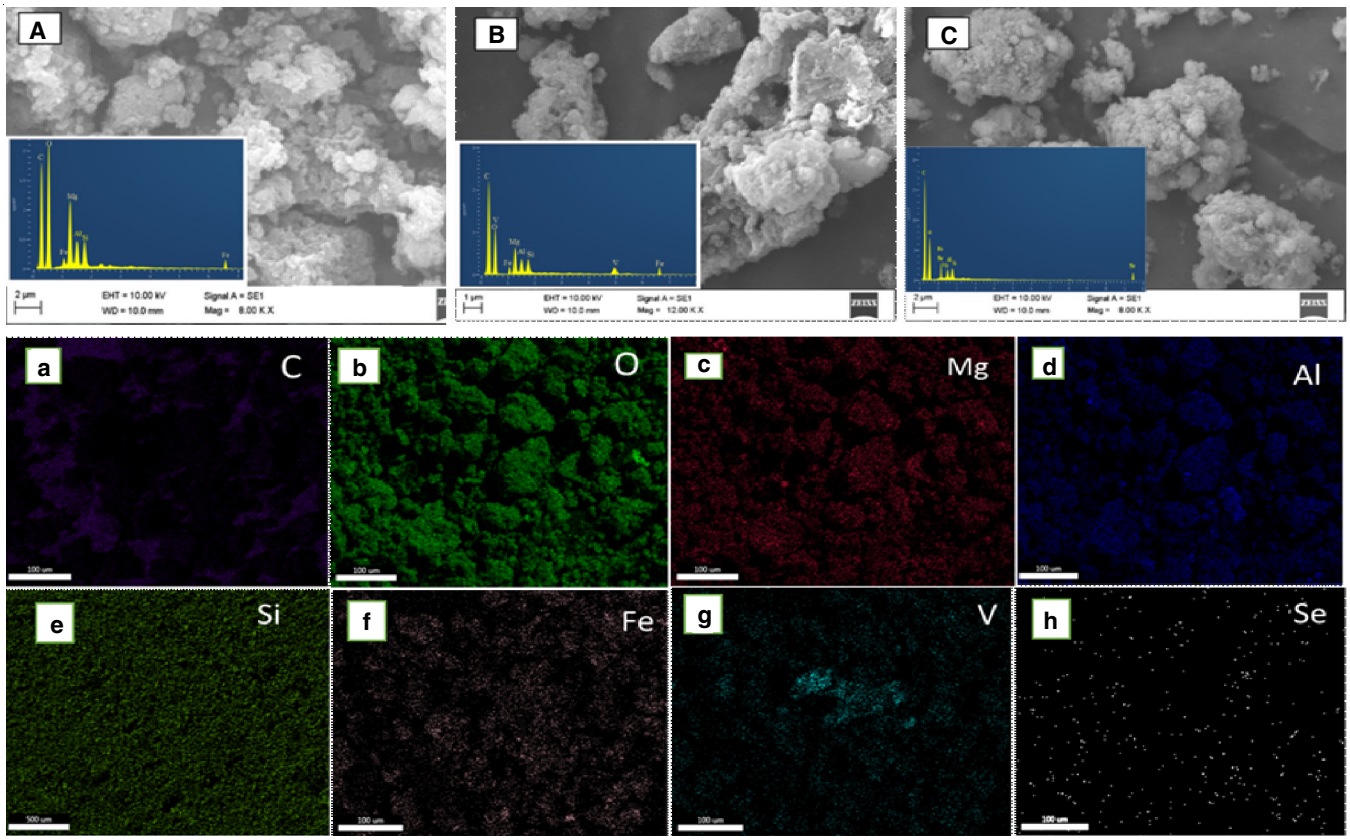

Fig. 5. SEM images of (A) Si-rGO/LDH-Fe (B) V(V)-loaded Si-rGO/LDH-Fe (C) Se(IV)-loaded Si-rGO/LDH-Fe. EDS elemental mapping of Si-rGO/LDH-Fe after V(V) and Se(IV) adsorption (a-h)

Fe. Batch adsorption experiments were conducted to investigate the effect of initial pH on the adsorption of V(V) and Se(IV) on Si-rGO/LDH-Fe at a pH ranging from 2.0-10.0. According to the speciation diagram (Fig. 6a and b), the anionic forms of V(V) ($H_2VO_4^-$ and HVO_4^{2-}) and Se(IV) ($HSeO_3^-$ and SeO_3^{2-}) exists at this pH range. As shown in Fig. 6c and d, the removal efficiency of Si-rGO/LDH-Fe presented a trend of increasing first and then declining with the increase of pH for both V(V) and Se(IV). The maximum removal efficiencies of V(V) and Se(IV) can be achieved at 5.5 and 5.0 with the values of 85 and 90%, respectively. At alkaline pH, a significant drop in the removal capacity of both species was observed due to increase of OH^- concentration, which competed with V(V) and Se(IV) oxyanions for the adsorption sites. Previous studies [33,34] also reported that Fe(III) oxide exhibit maximum binding capacity to V(V) and Se(IV) under acidic environment. The trend of V(V) and Se(IV) removal *versus* pH could be explained by the zeta potentials of adsorbent. As can be seen, the point of zero charge of Si-rGO/LDH-Fe was 5.6, at pH < 5.6 the reactive hydroxyl groups were strongly protonated (=Fe-OH_2^+), which favour the immobilization of oxyanions ($H_2VO_4^-$ and $HSeO_3^-$) on the surface of Si-rGO/LDH-Fe. These results convey a strong correlation between the sorption behaviour and solution pH during the adsorption process. In the optimized pH range the prominent V(V) and Se(IV) species (Fig. 6a-b) with the sorption sites illustrated as:

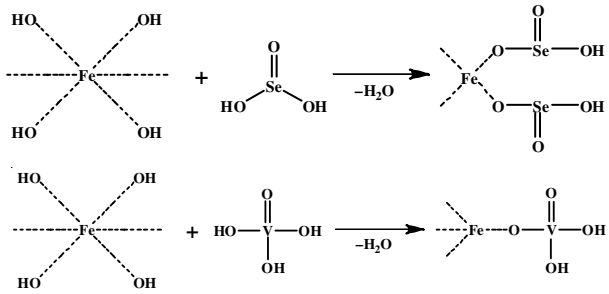

In Fig. 6c-d, the optimum pH for maximum adsorption of V(V) and Se(IV) was 5.5 and 5.0, respectively. The zeta potential value of Si-rGO/LDH-Fe at a pH of 5.5 and 5.0 was 2.02 mV and 11.97 mV, respectively which indicate ion exchange along with electrostatic attraction dominated the sorption process. According to the reported studies [35,36], surface hydroxyl groups play a critical role on the sorption of V(V) and Se(IV) onto Si-rGO/LDH-Fe and the sorption mechanism follows through inner sphere surface complexation *via* ligand exchange. The proposed mechanistic path for the sorption behaviour of of Si- rGO/LDH-Fe towards V(V) and Se(IV) is illustrated in **Scheme-I**.

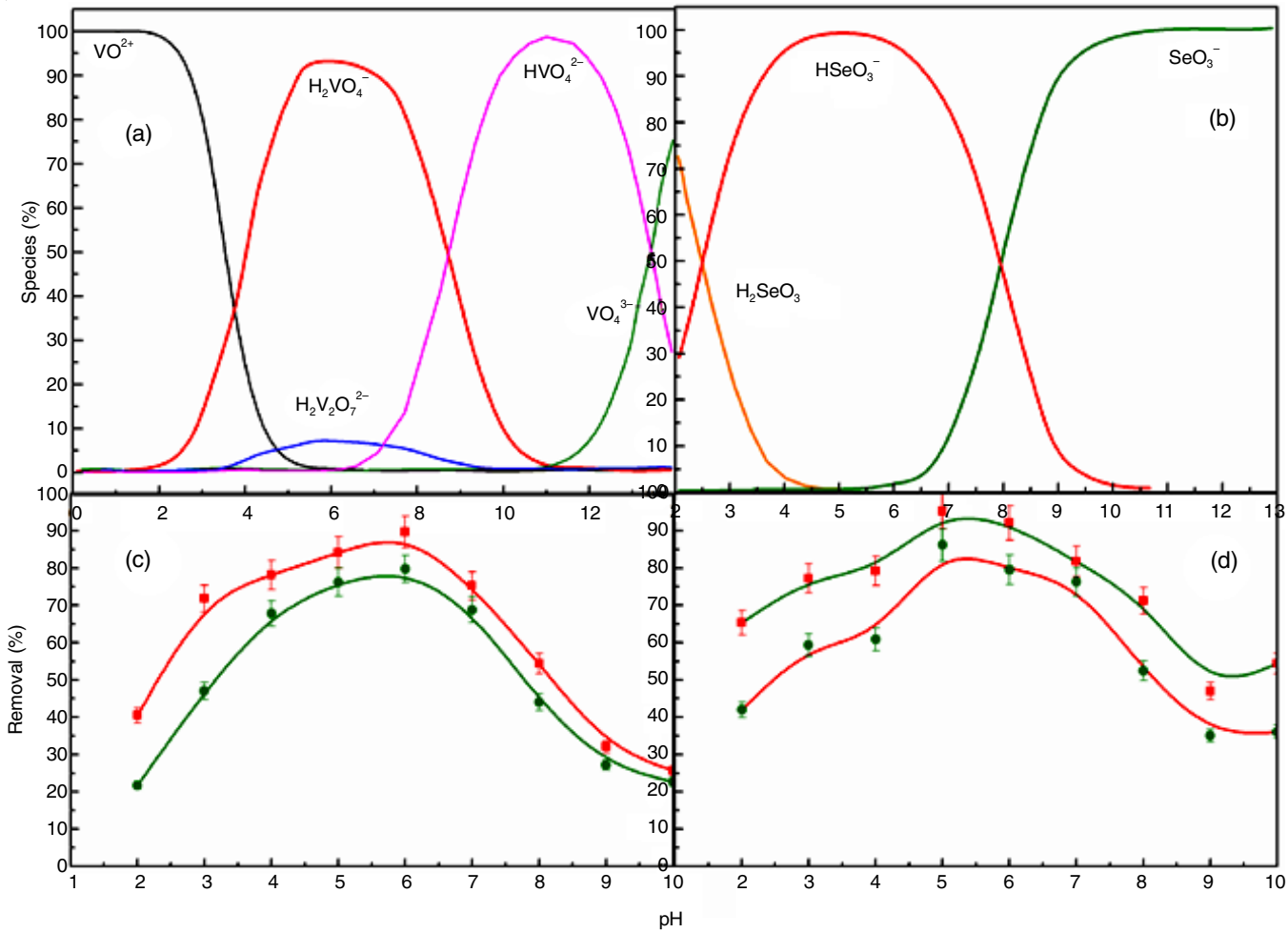

Fig. 6. Speciation of V(V) (a) and Se(IV) (b). Effect of pH on the adsorption of V(V) (c) and Se(IV) (d) onto Si-rGO/LDH-Fe

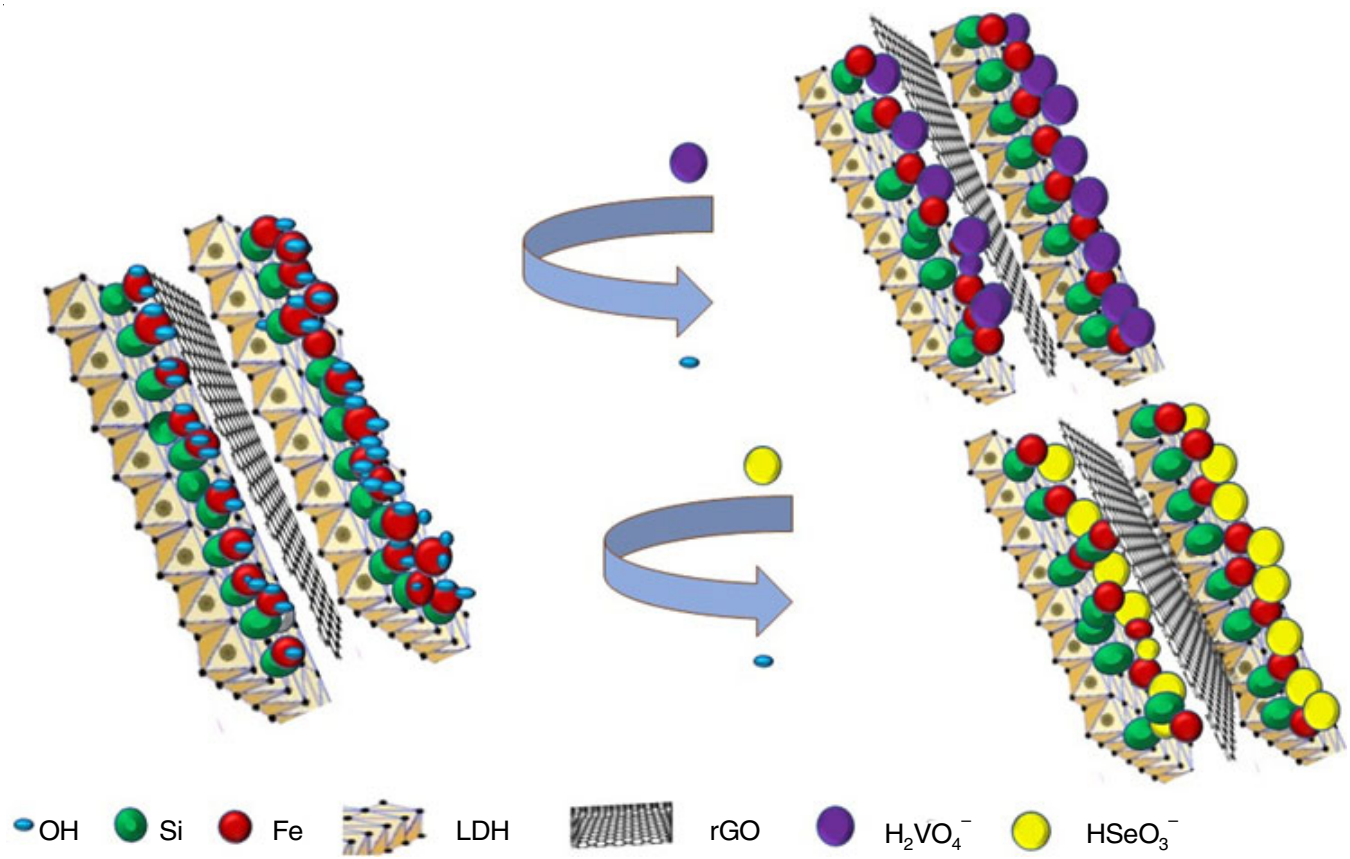

Scheme-I: Proposed mechanism for V(V) and Se(IV) adsorption onto Si-rGO/LDH-Fe

Equilibrium and kinetic studies: The adsorption isotherm studies were performed to describe the distribution of metal ions on the surface of adsorbent. The plots of the adsorption isotherms are shown in Fig. 7a and the equilibrium data were analyzed by using non-linear Langmuir, Freundlich and Sips isotherm models, respectively [37,38].

$$q_e = \frac{Q_o K_L C_e}{1 + K_L C_e} \quad (6)$$

$$q_e = K_F C_e^{1/n} \quad (7)$$

$$q_e = \frac{Q_s K_s C_e^{1/n_s}}{1 + K_S C_e^{1/n_s}} \quad (8)$$

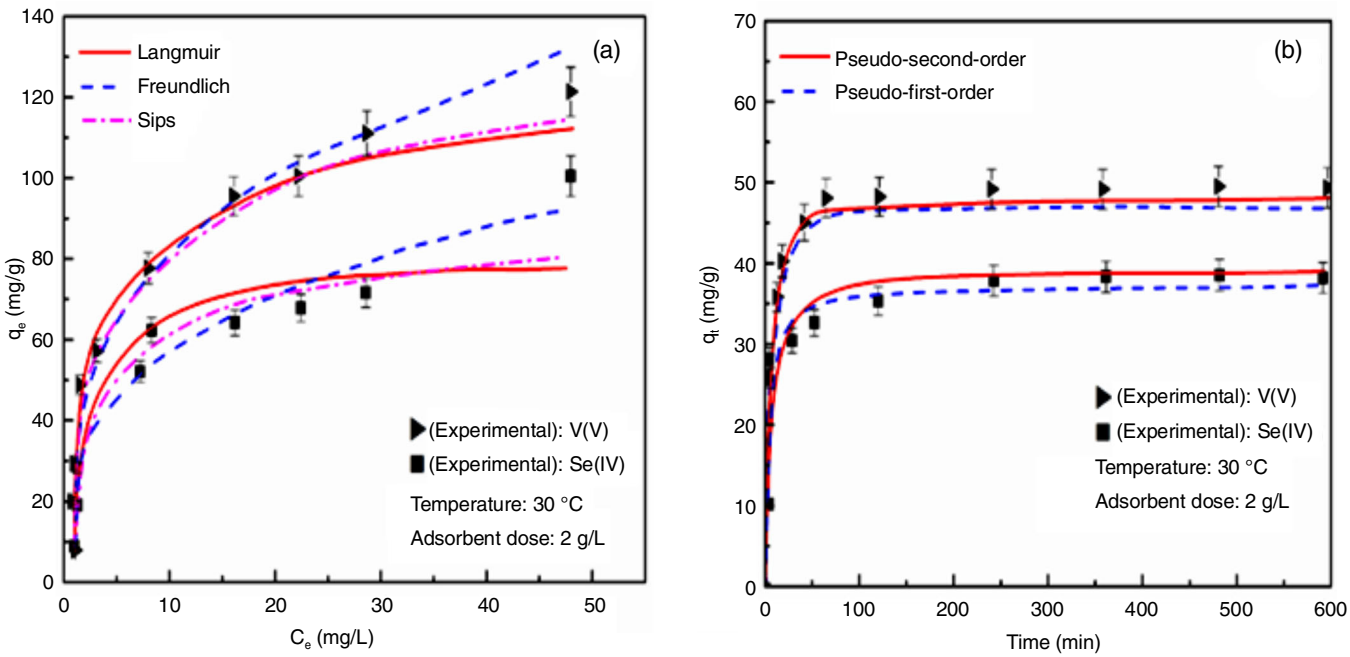

Fig. 7. Adsorption kinetics (A) and isotherm plots (B) of Se(IV) and V(V) on Si-rGO/LDH-Fe

TABLE-1
LANGMUIR, FREUNDLICH AND SIPS ISOTHERM PARAMETERS FOR THE ADSORPTION OF V(V) AND Se(IV) ONTO Si-rGO/LDH-Fe AT 30 °C

Metal ions	Langmuir				Freundlich				Sips				
	Q_0 (mg/g)	K_L (L/mg)	R^2	χ^2	K_F (mg^{1-n} $L^n g^{-1}$)	1/n	R^2	χ^2	Q_s (mg/g)	K_S (L/mg)	1/n	R^2	χ^2
V(V)	84.16	0.49	0.9982	1.34	39.43	0.223	0.982	11.21	87.26	0.96	0.312	0.98	1.86
Se(IV)	116.59	0.66	0.99	1.423	47.24	2.255	0.981	10.23	119.44	0.84	0.426	0.98	1.74

TABLE-2
KINETIC PARAMETERS OF Si-rGO/LDH-Fe ADSORPTION FOR V(V) AND Se(V)

Metal ions	$q_{e(exp)}$ (mg/g)	Pseudo-second-order				Pseudo-first-order			
		$k_2 \times 10^{-3}$ (g/mg/min)	$q_{e\,(cal)}$ (mg/g)	χ^2	R^2	$k_1 \times 10^{-2}$ (min^{-1})	$q_{e(cal)}$ (mg/g)	χ^2	R^2
V(V)	51.24	0.74	50.27	0.18	0.98	0.24	51.35	0.34	0.95
Se(IV)	42.23	0.87	41.11	0.11	0.99	0.14	43.41	0.53	0.93

where q_e (mg/g) is the amount of metal ions adsorbed at equilibrium, C_e (mg/L) is the equilibrium concentration of V(V) and Se(IV), Q_0 (mg/g) and Q_s represents maximum and specific adsorption capacity, 1/n is the heterogeneity coefficient, K_L, K_F and K_S represents adsorption energy, intensity of adsorption and Sips isotherm constant, respectively. The non-linear curve fitting with the experimental equilibrium data are listed in Table-1. The highest R^2 and lowest χ^2 values obtained after the non-linear regression analysis illustrate that theoretical Langmuir model was well fitted with the experimental data than Freundlich and Sips models. In all models the R^2 value beyond 0.90, which substantially indicate the favourability of three sorption models in explaining the adsorption mechanism.

The kinetic studies of metal ions onto Si-rGO/LDH-Fe were performed to evaluate the effect of concentration ranging from 50-250 mg/L during the sorption process. The kinetic experiments were carried out at a time interval 0-600 min and the reaction equilibrium were reached within 120 min. The adsorption rate was higher in the beginning due to the presence of large number of reaction sites available for the adsorption of V(V) and Se(IV). The kinetic data were analyzed using non-linear Lagergren pseudo-first-order and pseudo-second-order kinetic models and the results are shown in Fig. 7b.

Non-linear pseudo first order (eqn. 9) and second order (eqn. 10) models were used to fit the experimental data:

Pseudo-first-order model:

$$q_t = q_e(1 - e^{-k_1 t}) \quad (9)$$

Pseudo-second-order model:

$$q_t = \frac{k_2 q_e^2 t}{1 + k_2 q_e t} \quad (10)$$

where, q_e (mg/g) and q_t (mg/g) denotes the adsorption capacity of Si-rGO/LDH-Fe for V(V) and Se(IV) at equilibrium and time 't' respectively. k_1 (min^{-1}) and k_2 (g/mg/min) represents the adsorption rate constants of pseudo-first-order and pseudo-second-order model, kinetic parameters were estimated from the experimental data using non-linear curve fitting procedure and the results are given in Table-2.

The high regression coefficient R^2 [0. 98 for V(V) and 0.99 for Se(IV)] and the lower χ^2 [0.18 for V(V) and 0.11 Se(IV)] reflect a better correlation for pseudo-second-order model with the experimental data. With the increase of initial concentration, the sorption potential was increased, which indicated the dependency of sorption potential with the initial metal ion concentration.

Comparison of adsorbent materials: The sorption capacity of Si-rGO/LDH-Fe was compared with other reported materials towards V(V) and Se(IV). The maximum adsorption capacity for adsorbents depicted in the literature ranges from 16-94 mg/g for V(V) and 17-46 mg/g for Se(IV) (Table-3). Compared to these reported works Si-rGO/LDH-Fe shows much higher removal efficiency towards V(V) (116.59 mg/g) and Se(IV) (84.16 mg/g). The excellent decontamination performance of Si-rGO/LDH-Fe over the other materials was ascribed to the integrated effects associated with the rGO, LDH and Fe(III) oxide. The combination of LDH and rGO *via* effective crosslinking greatly inhibits the restacking of layers thereby providing large specific area and abundant active sites, which enhance sorption process.

TABLE-3
COMPARISON OF ADSORPTION CAPACITIES OF Si-rGO/LDH-Fe WITH OTHER ADSORBENTS REPORTED

Metal ions	Adsorbents	q_{max} (mg/g)	Ref.
V(V)	nZVI@LDH	93.7	[5]
	Fe-GWTR-P3	16	[14]
	PdO-MWCNTs	85	[39]
	MZ-PPY	65.0	[40]
	Si-rGO/LDH-Fe	116.59	Present study
Se(IV)	IS-50composite beads	17	[41]
	Magnetic Fe/Mn oxide	6.57	[42]
	MGO	45.57	[34]
	Calcined Mg-Fe LDH	45.6	[43]
	Si-rGO/LDH-Fe	84.16	Present study

Regeneration and reuse of Si-rGO/LDH-Fe: Recovery of the adsorbed metal ions and successful reusability of the composite material are significant in connection to the practical

applications of wastewater treatment. Desorption efficiency of the spent Si-rGO/LDH-Fe was evaluated using 0.01 M NaOH solutions having different concentration and the results are shown in Fig. 8. During the desorption process, the adsorption capacity decreases with respect to the four consecutive regeneration cycles from 97.8 to 77.84% and 98.58 to 69.03% for V(V) and Se(IV), respectively. The desorption capacity was also decreased from 95.56 to 71.07% and 83.12 to 58.56% for V(V) and Se(IV), respectively. The desorption capacity was also decreased to some extent due to the penetration of oxyanions into inner cavities of the prepared adsorbent material. These results illustrated the regeneration capacity and desorption efficiency of Si-rGO/LDH-Fe was consistent even after four consecutive cycles, which indicate the potential use of Si-rGO/LDH-Fe in water treatment applications.

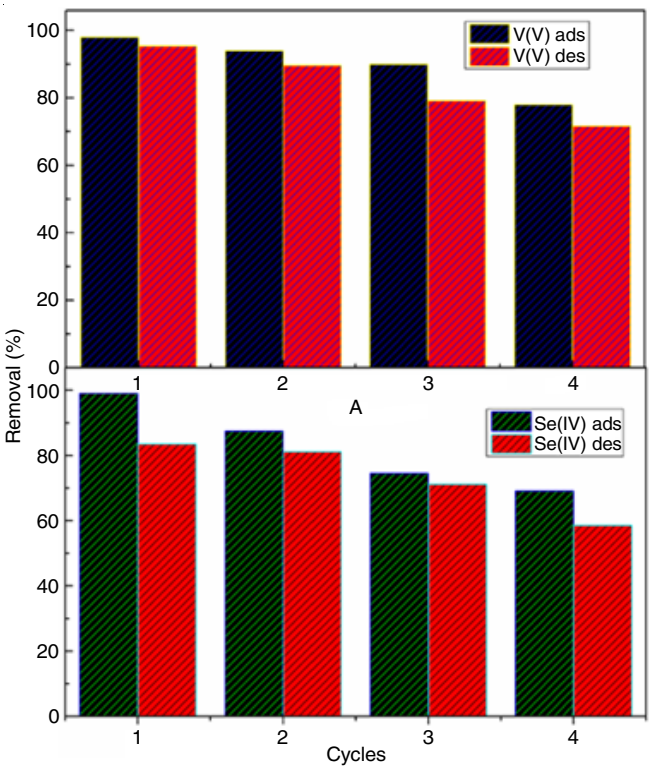

Fig. 8. Adsorption/desorption cycles of V(V) and Se(IV) for Si-rGO/LDH-Fe using 0.01 M NaOH

Conclusion

In this study, Si-rGO/LDH-Fe was prepared and evaluated for its sorption potential towards V(V) and Se(IV) ions. The prepared material was thoroughly characterized by various techniques and the results proved that the enhanced surface-active sites facilitate successful recovery of V(V) and Se(IV) from the aqueous systems. From the equilibrium studies, the maximum sorption potential was calculated to be 116.59 mg/g for V(V) and 84.16 mg/g for Se(IV). The corresponding non-linear curve fitting results was more consistent with the pseudo-second-order kinetic and Langmuir isotherm models with least χ^2 values. The novelty of the material was further confirmed by its consecutive performance in four cycles of adsorption-desorption experiments. These results revealed that Si-rGO/LDH-Fe was a potential candidate for the removal of V(V) and Se(IV) from the aqueous systems.

ACKNOWLEDGEMENTS

The authors are thankful to The Principal and The Head, Department of Chemistry, Sree Narayana College, Kollam, India for providing the laboratory facilities. One of the authors, S. Suma is grateful to University of Kerala, Trivandrum, India, for providing the research fellowship for carried out this work.

CONFLICT OF INTEREST

The authors declare that there is no conflict of interests regarding the publication of this article.

REFERENCES

1. X. Liu and L. Zhang, *Int. J. Biol. Macromol.*, **79**, 110 (2015); https://doi.org/10.1016/j.ijbiomac.2015.04.065
2. C.M. Gonzalez, J. Hernandez, J.R. Peralta-Videa, C.E. Botez, J.G. Parsons and J.L. Gardea-Torresdey, *J. Hazard. Mater.*, **211-212**, 138 (2012); https://doi.org/10.1016/j.jhazmat.2011.08.023
3. H. Liu, B. Zhang, H. Yuan, Y. Cheng, S. Wang and Z. He, *Environ. Pollut.*, **231**, 1362 (2017); https://doi.org/10.1016/j.envpol.2017.08.111
4. V.K. Sharma, M. Sohn and T.J. McDonald, Eds.: S. Ahuja, Remediation of Selenium in Water: A Review. In Advances in Water Purification Techniques; Meeting the Needs of Developed and Developing Countries, Elsevier: Amsterdam, The Netherlands, Chap. 8, pp. 203-218 (2019).
5. X. Kong, J. Chen, Y. Tang, Y. Lv, T. Chen and H. Wang, *J. Hazard. Mater.*, **392**, 122392 (2020); https://doi.org/10.1016/j.jhazmat.2020.122392
6. G. Zelmanov and R. Semiat, *Sep. Purif. Technol.*, **103**, 167 (2013); https://doi.org/10.1016/j.seppur.2012.10.037
7. L. Wang, C. Shi, L. Wang, L. Pan, X. Zhang and J.-J. Zou, *Nanoscale*, **12**, 4790 (2020); https://doi.org/10.1039/C9NR09274A
8. E.A. Campos, D.V.B.S. Pinto, J.I.S. de Oliveira, E. da Costa-Mattos and R. de Cássia Lazzarini Dutra, *J. Aerosp. Technol. Manag.*, **7**, 267 (2015); https://doi.org/10.5028/jatm.v7i3.471
9. S. Periyasamy, P. Manivasakan, C. Jeyaprabha, S. Meenakshi and N. Viswanathan, *Int. J. Biol. Macromol.*, **132**, 1068 (2019); https://doi.org/10.1016/j.ijbiomac.2019.03.232
10. T. Wen, X. Wu, X. Tan, X. Wang and A. Xu, *ACS Appl. Mater. Interfaces*, **5**, 3304 (2013); https://doi.org/10.1021/am4003556
11. W. Sun, T. Wu, L. Wang, C. Dong and G. Liu, *Ind. Eng. Chem. Res.*, **58**, 16516 (2019); https://doi.org/10.1021/acs.iecr.9b01742
12. H. Pang, Y. Wu, X. Wang, B. Hu and X. Wang, *Chem. Asian J.*, **14**, 2542 (2019); https://doi.org/10.1002/asia.201900493
13. Q. Tao, H. He, R.L. Frost, P. Yuan and J. Zhu, *Appl. Surf. Sci.*, **255**, 4334 (2009); https://doi.org/10.1016/j.apsusc.2008.11.030
14. A. Khan, J. Wang, J. Li, X. Wang, Z. Chen, A. Alsaedi, T. Hayat, Y. Chen and X. Wang, *Environ. Sci. Pollut. Res.*, **24**, 7938 (2017); https://doi.org/10.1007/s11356-017-8388-8
15. V. Georgakilas, M. Otyepka, A.B. Bourlinos, V. Chandra, N. Kim, K.C. Kemp, P. Hobza, R. Zboril and K.S. Kim, *Chem. Rev.*, **112**, 6156 (2012); https://doi.org/10.1021/cr3000412
16. C.M. Par, D. Wang, J. Heo, N. Her and C. Sud, *J. Nanopart. Res.*, **20**, 93 (2018); https://doi.org/10.1007/s11051-018-4202-x
17. M. Tian, C. Liu, Z.G. Neale, J. Zheng, D. Long and G. Cao, *ACS Appl. Mater. Interfaces*, **11**, 35977(2019); https://doi.org/10.1021/acsami.9b10719

18. K.-H. Goh, T.T. Lim and Z. Dong, *Water Res.*, **42**, 1343 (2008); https://doi.org/10.1016/j.watres.2007.10.043
19. W.S. Hummers Jr. and R.E. Offeman, *J. Am. Chem. Soc.*, **80**, 1339 (1958); https://doi.org/10.1021/ja01539a017
20. X. Sun, E. Neuperger and S.K. Dey, *J. Colloid. Interface Sci.*, **459**, 264 (2015); https://doi.org/10.1016/j.jcis.2015.07.073
21. O. Akhavan, E. Ghaderi, S. Aghayee, Y. Fereydooni and A. Talebi, *J. Mater. Chem.*, **22**, 13773 (2012); https://doi.org/10.1039/c2jm31396k
22. D. Fu, Z. He, S. Su, B. Xu, Y. Liu and Y. Zhao, *J. Colloid Interface Sci.*, **505**, 105 (2017); https://doi.org/10.1016/j.jcis.2017.05.091
23. A. Yürüm, Z.O. Kocabaþ-Atakli, M. Sezen, R. Semiat and Y. Yürüm, *Chem. Eng. J.*, **242**, 321 (2014); https://doi.org/10.1016/j.cej.2014.01.005
24. L. Deng, H. Zeng, Z. Shi, W. Zhang and J. Luo, *J. Colloid Interface Sci.*, **521**, 172 (2018); https://doi.org/10.1016/j.jcis.2018.03.040
25. L.V. Tan, H.T. Nguyen Thi, T.U. Dao Thi and V.T. Tran, *Asian J. Chem.*, **32**, 2381 (2020); https://doi.org/10.14233/ajchem.2020.22481
26. A.S. Murali and J. Rajendran, *Asian J. Chem.*, **32**, 1557 (2020); https://doi.org/10.14233/ajchem.2020.22647
27. J. Zhu, P. Yuan, H. He, R. Frost, Q. Tao, W. Shen and T. Bostrom, *J. Colloid Interface Sci.*, **319**, 498 (2008); https://doi.org/10.1016/j.jcis.2007.11.037
28. H. Zhang, J. Zhang, R. Yun, Z. Jiang, H. Liu and D. Yan, *RSC Adv.*, **6**, 34288 (2016); https://doi.org/10.1039/C6RA04398D
29. N. Tian, X. Tian, X. Liu, Z. Zhou, C. Yang, L. Ma, C. Tian, Y. Li and Y. Wang, *Chem. Commun.*, **52**, 11955 (2016); https://doi.org/10.1039/C6CC05659H
30. W. Sun, W. Pan, F. Wang and N. Xu, *Chem. Eng. J.*, **273**, 353 (2015); https://doi.org/10.1016/j.cej.2015.03.061
31. Q. Huang, Y. Chen, H. Yu, L. Yan, J. Zhang, B. Wang, B. Du and L. Xing, *Chem. Eng. J.*, **341**, 1 (2018); https://doi.org/10.1016/j.cej.2018.01.156
32. R. Zhang, T. Leiviskä, J. Tanskanen, B. Gao and Q. Yue, *Chem. Eng. J.*, **361**, 680 (2019); https://doi.org/10.1016/j.cej.2018.12.122
33. R. Geng, W. Wang, Z. Din, D. Luo, B. He, W. Zhang, J. Liang, P. Li and Q.J. Fan, *J. Mol. Liq.*, **309**, 113029 (2020); https://doi.org/10.1016/j.molliq.2020.113029
34. Y. Fu, J. Wang, Q. Liu and H. Zeng, *Carbon*, **77**, 710 (2014); https://doi.org/10.1016/j.carbon.2014.05.076
35. N. Chubar, *J. Mater. Chem. A Mater. Energy Sustain.*, **2**, 15995 (2014); https://doi.org/10.1039/C4TA03463E
36. C.L. Peacock and D.M. Sherman, *Geochim. Cosmochim. Acta*, **68**, 1723 (2004); https://doi.org/10.1016/j.gca.2003.10.018
37. R. Sreenivasan, S. Suma Mahesh and V.S. Sumi, *Sep. Sci. Technol.*, **54**, 1453 (2019); https://doi.org/10.1080/01496395.2018.1534868
38. T.S. Anirudhan, J.R. Deepa and J. Christa, *J. Colloid Interface Sci.*, **467**, 307 (2016); https://doi.org/10.1016/j.jcis.2016.01.023
39. V.K. Gupta, A. Fakhri, A.K. Bharti, S. Agarwal and M. Naji, *J. Mol. Liq.*, **234**, 117 (2017); https://doi.org/10.1016/j.molliq.2017.03.061
40. N.H. Mthombeni, S. Mbakop, A. Ochieng and M.S. Onyango, *J. Taiwan Inst. Chem. Eng.*, **66**, 172 (2016); https://doi.org/10.1016/j.jtice.2016.06.016
41. M. Li, A. Dopilka, A.N. Kraetz, H. Jing and C.K. Chan, *Ind. Eng. Chem. Res.*, **57**, 4978 (2018); https://doi.org/10.1021/acs.iecr.8b00466
42. C.M. Gonzalez, J. Hernandez, J.G. Parsons and J.L. Gardea-Torresdey, *Microchem. J.*, **96**, 324 (2010); https://doi.org/10.1016/j.microc.2010.05.005
43. J. Das, B. Sairam Patra, N. Baliarsingh and K.M. Parida, *J. Colloid Interface Sci.*, **316**, 216 (2007); https://doi.org/10.1016/j.jcis.2007.07.082